EPTT 2024
Escola de Primavera de Transição e Turbulência

ABCM
Associação Brasileira de Engenharia e Ciências Mecânicas

EPTT-2024-XXXX
SOME EXPERIMENTAL RESULTS OF THE IMPACT CAUSED BY A RECTANGULAR BUMP ON BOUNDARY LAYER TRANSITION

Lenz J. L. Lazaro
Victor B. Victorino
São Carlos School of Engineering, University of São Paulo - Av. Trabalhador São Carlense, 440. Zip code: 13566-590
lenzjll@usp.br
barcelos.victorino@usp.br

Marcello A. F. Medeiros
São Carlos School of Engineering, University of São Paulo - Av. Trabalhador São Carlense, 440. Zip code: 13566-590
marcello@sc.usp.br

Abstract. *The study of surface irregularities is an important topic in the aeronautical field. Various approaches have been reviewed over time, integrating semi-empirical theories to anticipate and explain the behavior of the boundary layer under these conditions. In this paper will be seen some experimental results of the effects caused by rectangular bump on the transition from laminar to turbulence of the boundary layer, where this single roughness is placed at a certain distance from the leading edge of a flat plate with a little pressure gradient. The experiments were carried out at the Low Acoustic Noise and Turbulence (LANT) wind tunnel from the School of Engineering of São Carlos, University of São Paulo. This documentation shows how the amplification of Tollmien-Schlichting waves is significantly affected by different bump heights and free stream velocities. Furthermore, it will be shown that for determined bump heights, an abrupt transition of the boundary layer is reveled.*

Keywords: *Boundary layer transition, bypass transition, Tollmien–Schlichting wave, rectangular bump*

1. INTRODUCTION

The behavior of the transition from laminar to turbulent flow is strongly influenced by various type of surface irregularities, such as steps, cavities, and protrusions, which are commonly encountered in practice. These imperfections are analyzed applying different approaches in various fields of the aeronautic for aerodynamic applications, this includes cases where these surface imperfections on an aircraft lead to anticipate the transition to turbulence and consequently causing a drastic increase in the total drag coefficient.

The motivation behind this paper is the reduction of the drag coefficient in aircraft, which will bring significant benefits to the aerospace industry. Important estimates provided by Schneider (2001) quantify that a hypothetical 1% reduction in the total drag of a large commercial aircraft operating over long distances would result in savings of $400,000$ liters of fuel and a reduction of $5,000$ kg of harmful emissions per year. Hence, a substantial reduction in fuel consumption can be achieved in commercial aircraft, leading to lower costs associated with fuel consumption. Additionally, the aircraft's payload can be dramatically increased, resulting in improved performance and increased flight range. According to Reneaux (2004), approximately 22% of airline costs are attributed to fuel consumption. Schrauf (2005) establish that the friction constitutes more than half of the total aircraft drag, with 28% for wing and about 22% on the fuselage.

For this reason, this research is related to the instability and transition on boundary layer due to several disturbances and viscous effects. Tollmien (1928) and Schlichting (1933) worked on the development of the linear stability theory, which is based on the viscous instability of the laminar boundary layer of Blasius profile for small-amplitude disturbances. From this perspective, Schubauer and Skramstad (1947) were the first to experimentally demonstrate that transition is dominated by the growth of T-S waves. Their experiment confirmed the existence of T-S waves, their connection to transition, and the quantitative description of their behavior. On the other hand, the transition prediction studied by van Ingen (1956) and Smith and Gamberony (1956) correlated experimental results with linear stability theory. As a result, they developed the e^N method, capable of predicting transition when the integral growth of T-S waves reaches a factor of $N = 9$, thus achieving an estimated value of reference.

As mentioned above, there are elements that cause instability in the boundary layer, so the initial experimental studies of the effects of surface roughness were addressed by Tani *et al.* (1940), Stuper (1949), and Dryden (1953). These experiments demonstrated the influence of the roughness height on the transition Reynolds number, which is upstream displacement as the roughness height increases. Klebanoff and Tidstrom (1972) indicated that these imperfections have a destabilizing effect in the recovery region, i.e., the region of the distorted mean flow immediately downstream of the roughness element. This leads to the transition occurring upstream compared to the case without roughness. Results from Wang and Gaster (2005) demonstrated that backward-facing steps are more destabilizing compared to forward-facing steps. Furthermore, there are a phenomena that deviate from the growth of T-S waves and are thus referred to as bypass transition called after by Morkovin (1985). Besides Reshotko (2001) said that bypass transition is inherently nonlinear.

The present study aims to experimentally examine the influence of a rectangular bump, with variable height on boundary layer transition. Initially, static pressure distribution on the wall were measured for the smooth case (no bump) to ensure the gradient pressure is small, and to verify this, Blasius profiles were measured. Afterwards, a Preston tube was used to determine the transition point which is compared with the spectra velocities measured by hot wire anemometer. In addition, to mapping the T-S wave evolution, velocity fluctuation acquisitions were taken within the boundary layer, later the fast Fourier transform is applied in order to observe the dominated bands of the T-S waves and comparing with the Orr-Sommerfeld solution. A single curve analyzed by Tani and Hama (1945) using a circular roughness will be compared with results obtained from rectangular bumps showing a similar relation. Finally, it will be reveled an important numerical result about the quadratic behavior of the T-S waves with respect to relatively small bump heights and as well as the concordance of the amplification factor theory and an experimental result for the smooth case.

2. EXPERIMENTAL PROCEDURE

The experiments were conducted in the Low Aeroacoustic Noise and Turbulence Wind Tunnel (LANT) at EESC-USP. The closed circuit wind tunnel has a test section with transverse dimensions of 1.00 m $\times$ 1.00 m and a length of 3.00 m. To carry out experiments of transition is very important to know the turbulent intensity of the free stream. Hence, in Tab. 1, it can be observed that, for different free-stream flow velocities measured inside the empty test section and with the model installed, turbulence intensities vary slightly within a frequency range from 1 to 1024 Hz. Furthermore, in Fig. 1 is displayed turbulence that is compared with another two tunnels presented by Gaster (1990) and Klebanoff and Tidstrom (1972). It could be seen that LANT is more similar to Klevanoff's wind tunel, except for the noise evidenced at frequencies greater than 100 Hz. For this, several devices can be found within LANT to enhance flow uniformity, reduce turbulence intensity and background acoustic noise. A detailed overview of the design and performance of the LANT wind tunnel is provided in Amaral (2021). Also a curve was fitted to represent the relation between the source's revolution per minutes and the maximum free stream velocity in the test section. Figure 2 exhibits a range of available velocities to conducting transition experiments in which (blue line as linear fit) is with installed model and (dashed lines) is when the test section is empty.

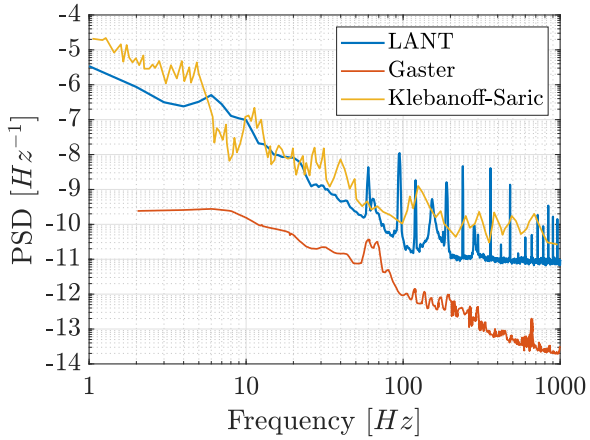

Figure 1: Power spectral density of turbulence intensity in the test section compared with similar tunnels.

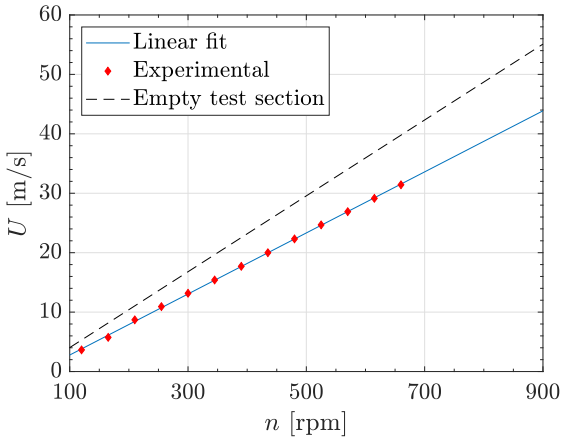

Figure 2: Velocity in relation to the fan's number of revolutions.

Inside the test section, a flat plate model made of aluminium was installed, in Fig. 2 is shown the upper view of the airfoil model and it is positioned vertically in the test section. The dimensions of the working surface (flat plate) are 2000 (chord) mm $\times$ 1000 (span) mm, attached to an asymmetrical leading edge Hanson *et al.* (2012). A fairing profile on the back side was used to cover all the mechanisms, this is suppoted by softwares MSES and XFOIL Drela and Giles (1987) Moreover, two control surfaces a flap and tab are attached to the model's trailing edge, these elements allow fine-tuning of the pressure distribution.

Table 1: Free-stream turbulence intensity measured under different conditions.

U_∞ **[m/s]**	Tu **%**	**Frequency Range [Hz]**	**Test Section**
10	0,041	1 - 1024	Empty
15	0.040	1 - 1024	Empty
20	0.038	1 - 1024	Empty
27	0.077(0.054)	1 - 1024(4 - 1024)	Installed Model

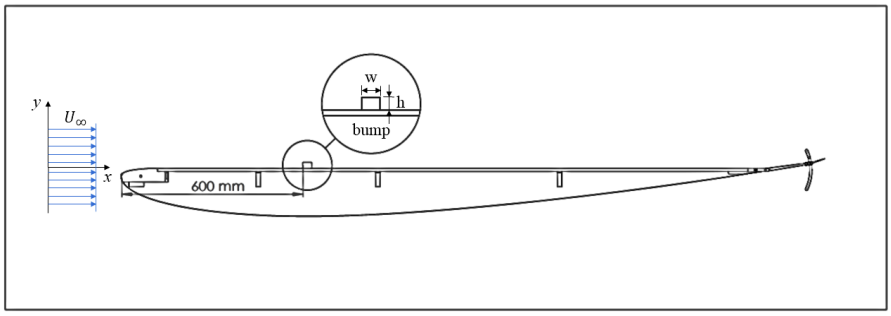

Figure 3: Top view of the flat plate model with installed rectangular bump.

The interchangeable protrusion system in Fig. 4, coupled to the flat plate to 600 mm from the leading edge, houses the mechanisms needed to alter the geometry. The bump measures 30 mm in length and 600 mm in span-wise with a adjustable height of 20 mm that can be moved inwards to create a gap or outwards to create a bump.

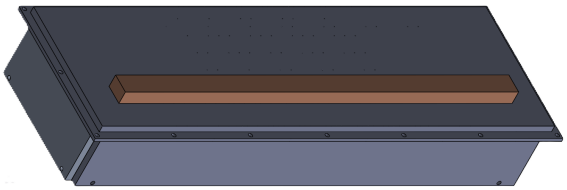

Figure 4: Device that conforms to the roughness element (rectangular bump).

To estimate the transition location, a round Preston tube with a diameter of 0.9 mm Fig. 6 was used to measure the total pressure close to the wall. This measurement is proportional to the skin friction coefficient. This method was proposed by Preston (1954), in which utilizes stagnation pressure information derived from a tube placed on the wall. Afterward, this instrument was used to determent the transition location, as utilised after Tani *et al.* (1940), Schubauer and Skramstad (1947), Klebanoff and Tidstrom (1972) e Crouch and Kosorygin (2020) to detect transition due to different roughness elements heights. Therefore, the minimum value of dynamical pressure distribution within the laminar regime represents the location of the transition. Furthermore, a wing model was designed to cover the rod, specifically adapted to house the Pitot tube, Preston tube and HWA probe. The wing also covers the pneumatic hoses of both devices, in Fig. 5 below, a clear view of the assembly is shown. The needle of the Preston tube was bent towards the flat plate, similar to the HWA probe, and positioned with a slight angle of contact with the flat plate. By using an LVDT (Linear Variable Differential Transformer) distance sensor installed at the tip of the wing, it was possible to maintain a constant angle of the needle across different runs. The sensitive element consists of a Honeywell TruStability differential pressure sensor, model 004ND, which has a total error range of 4.97 Pa. The sensor is connected to an Arduino board, and the data is read by a MATLAB function.

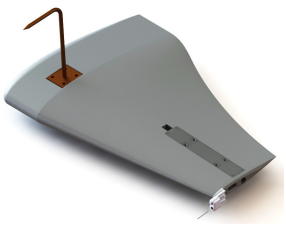

Figure 5: Wing model houses devices.

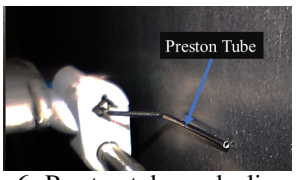

Figure 6: Preston tube probe lies on the plate surface.

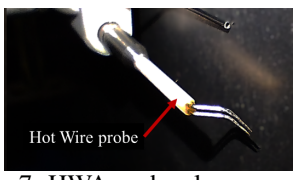

Figure 7: HWA probe close to the wall.

Hot-Wire Anemometry was the chosen technique for velocity fluctuation measurements. The anemometer circuit used was the AN-1002 from A.A. Lab System, and the hot wire probe Fig. 7, was the miniature wire boundary layer probe 55P15 from Dantec Dynamics. The voltage signal is derived and sent to two data acquisition modules, one for mean velocity (DC voltage) and the other for fluctuating velocity (AC voltage). The first one is a National Instruments USB-DAQ 6002 with 16-bit resolution and a maximum sampling rate of up to 50 kSamples/s on the analog input channels and 5 kSamples/s on the analog output channels. The second one consists of a set of 7 PXI-4496/98 boards with 24-bit resolution installed in a PXI-1042Q chassis, all from National Instruments. While these boards are used for data acquisition from microphones, one of them is used for recording fluctuating velocity due to its better resolution compared to the USB-DAQ 6002. Signal conditioning and manipulation were performed using MATLAB. To place the probes within the test section along the flat plate was controlled by a three-axis positioning mechanism.

3. SOME RESULTS

To start, was demonstrate in this experiment that the flat plate follows the Blasius boundary layer profile. For this experiment, an anemometer was used, but before was employed a calibration of the voltage and velocity Fig. 8. The conversion from voltage to velocity was done using King's Law, $E^2 = A + BU^n$, where A, B, and n are constants obtained from the least-squares regression. For this calibration a calculated function was given by $U = ((E^2 + 1.89)/2.31)^{\frac{1}{0.58}}$,

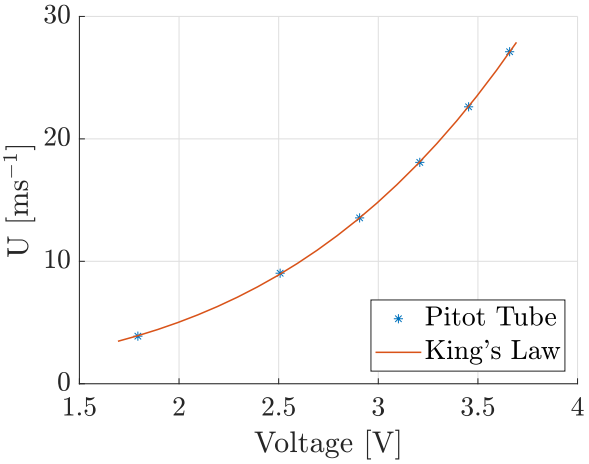

Figure 8: Velocity calibration using king's law.

To plot the velocity profile were taken 41 steps along the y-axis of 0.2 mm for different x-stations. The data acquisition time was 8 seconds per step with a sampling rate of 2048 Hz. Then, a graph of η against normalized velocity U/U_∞ was plotted, where $\eta = y\sqrt{U_\infty/\nu x}$. The flow passing through the flat plate behaves in a laminar way for velocities of 17 m/s, 26 m/s and 28 m/s for $x = 0.4$ m, $x = 0.6$ m, and $x = 1.0$ m as display Fig. 9 respectively. Let us observe that the experimental results closely match the theoretical curve derived from the Blasius equation solution.

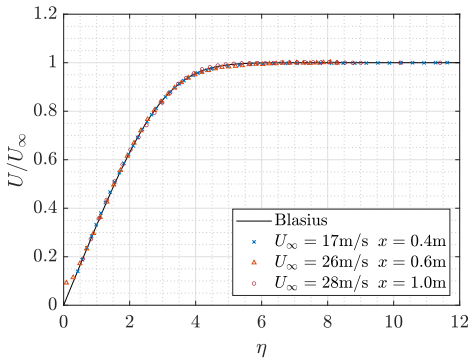

Figure 9: Normalized velocity profiles at different places on the plate, compared with the theoretical Blasius profile.

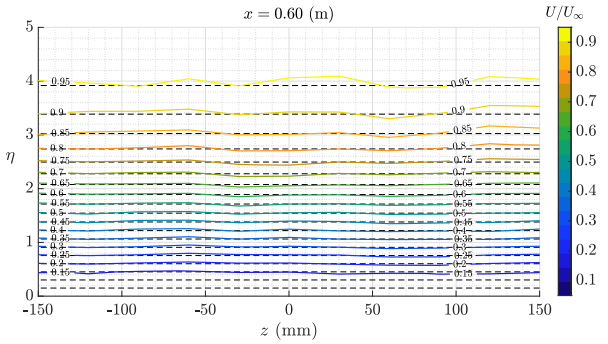

Figure 10: Contours of the non-dimensional η values, showing the two-dimensionality of the Blasius profiles on the plate along z at $x = 600$ mm.

We now move on to the results obtained on the span-wise of the plate, which will give us guarantee regarding the parametric space that can be useful and the region up to which the tunnel's boundary layer has an effect. We will then verify that there is a region that behaves evenly and also exhibits symmetry concerning the center-line of the plate. As

shown in Fig. 10, the values of η in relation to z are displayed at the position $x = 600$ mm, where roughness element is located. We see that at least up to 65% of the free-stream velocity, an appropriate uniformity is presented within the interval of interest, where the signals are collected for subsequent analysis of the evolution of T-S waves, which is the zone where these waves are captured with the best spectral visibility.

3.1 Transition location

The transition location was determined using a Preston tube technique as described on the previous section, this is moved along the x direction, where the probe is situated on the centerline of the flat plate i.e in the middle of the span (z-axis). The total pressure measured by the instrument is related to the velocity profile near the wall. The transition location is determined based on the distribution of the minimum total pressure. The free-stream velocity was 27.3 m/s, and the Reynolds number based on the displacement thickness over the smooth plate for $x = 630$ mm (where the bump begins) was $Re_{\delta^\star} = 1635$. The Preston tube is then placed into contact with the plate wall, starting the sweep at $x = 640$ mm to 1900 mm discredited into 31 steps. For the smooth surface, it can be observe that the natural transition occurred at 1900 mm Fig. 11 while for $h = 0.2$ mm and $h = 0.4$ mm the transition location moves to $x = 1800$ mm and $x = 1700$ respectively, already for $h = 0.6$ mm and $h = 0.8$ mm the transition point walked further upstream showing an evident change of transition. Figure 12 exhibit what happen when $h = 2$ mm up to $h = 20$ mm. Here, we can observe that the transition does not occur, but a decreasing of the dynamical pressure therefore the skin friction coefficient for each case is reveled. Moreover, close to the bump, the pressure measured becomes negative as the bump height increases, this could be due to a phenomenon known as separation bubble.

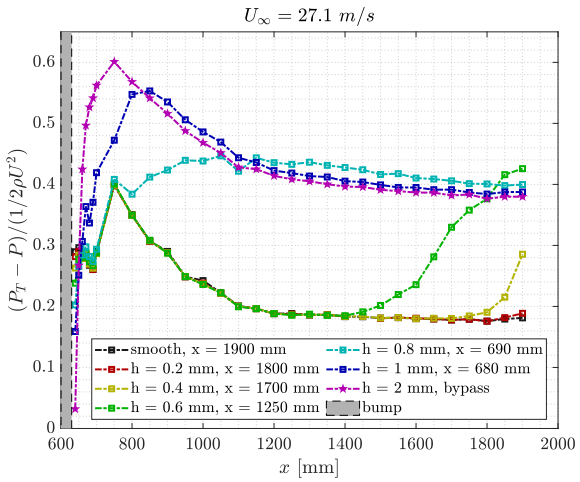

Figure 11: Transition location is determined for T-S regime.

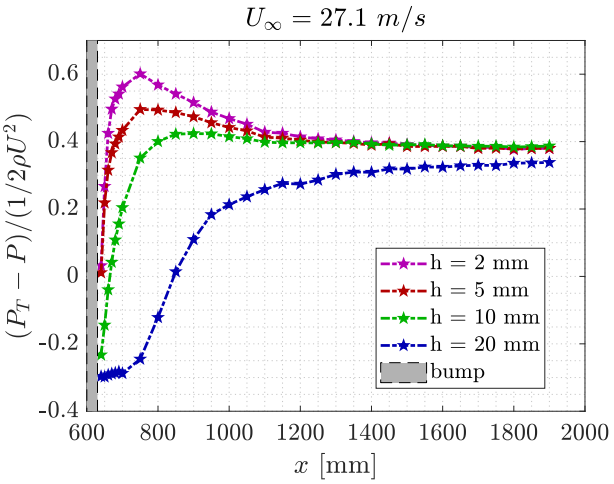

Figure 12: Bypass transition caused by larger bumps.

3.2 Spectra of velocity fluctuation

The velocity fluctuation signal was measured using hot-wire anemometer probe. The probe was positioned within the boundary layer at a distance from the surface such that the mean velocity is approximately 40% of the free-stream velocity. To achieve this, the anemometer was calibrated in order to accurately determine this value, resulting in several y-position for each x-station due to the increasing boundary layer thickness along the length of the flat plate. This calibration was based on the Blasius profile experiment explained above. For post-processing of the signal, the Welch method, involving the averaging of spectra from subsets of the time signal, this was employed to reduce spurious noise.

For this case, the data acquisition was carried out in a free stream velocity of 27.34 m/s and was performed at 16 points along the flat plate. It began at $x = 640$, which is 10 mm from the trailing edge of the bump, and extended up to $x = 1900$ mm, close to the end of the model. These points were spaced at 100 mm steps, starting at $x = 700$, except for the first two points as shown in Fig. 15. The data acquisition lasted for 8 seconds with a sampling resolution of 8192 Hz.

In Fig. 13 a). and b). represent a acquired signal of 1 second, where time t [s] is plotted against velocity fluctuation u' [m/s]. We can see that the natural transition of the boundary layer occurs at 1900 mm that is $Re = 2927$ and for $h = 0.4$ mm the transition takes place at 1700 mm exhibiting a significant change. These stations were chose for their intermittent nature. The variables showed in the following graphs Fig. 14 a). and Fig. 15 a)., are x (distance), f (frequency), and $\mathcal{F}(u'/U_\infty)$, which represents the fast Fourier transform. These graphs were compared with the Orr-Sommerfeld solution, which Reynolds delta star $Re_{\delta^\star}$ is plotted versus dimensionless frequency $F = 2\pi f\nu/U_\infty^2 \times 10^6$. For the smooth case Fig. 14 b)., the Fourier transform exhibits dominant bands between 51 Hz and 432 Hz, whose frequencies are equivalent to $F = 7.7$ and $F = 66.3$ from the instability region Fig. 15 b)., and where it is identified that these frequencies delimited for

this points (blue and red) reveled the dominant bands of the T-S waves. The amplification of the TS waves is progressive along x, showing that in the transition regime of the boundary layer, all low and high frequencies bands start to amplify, causing this dominant band to be submerged among them. For the case with $h = 0.4$ mm Fig. 17 and Fig. 18, it can be noticed that this evolution was slightly more intense, with the spectra starting to become turbulent, indicating the onset of boundary layer transition just at $Re_{\delta^\star} = 2768$.

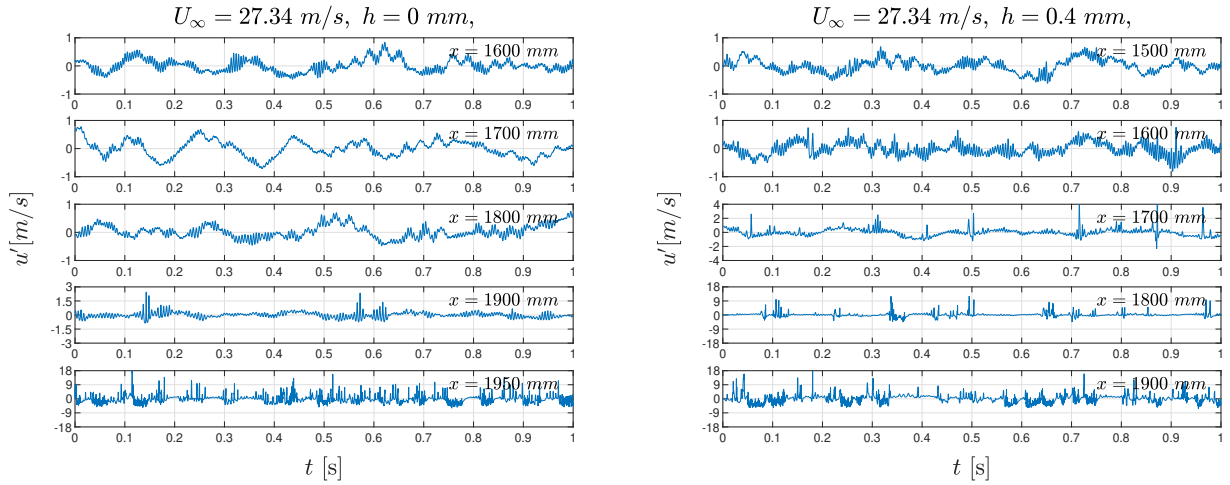

a). $h/\delta_h^\star = 0$. b). $h/\delta_h^\star = 0.36$.

Figure 13: Oscillogram of the velocity fluctuations.

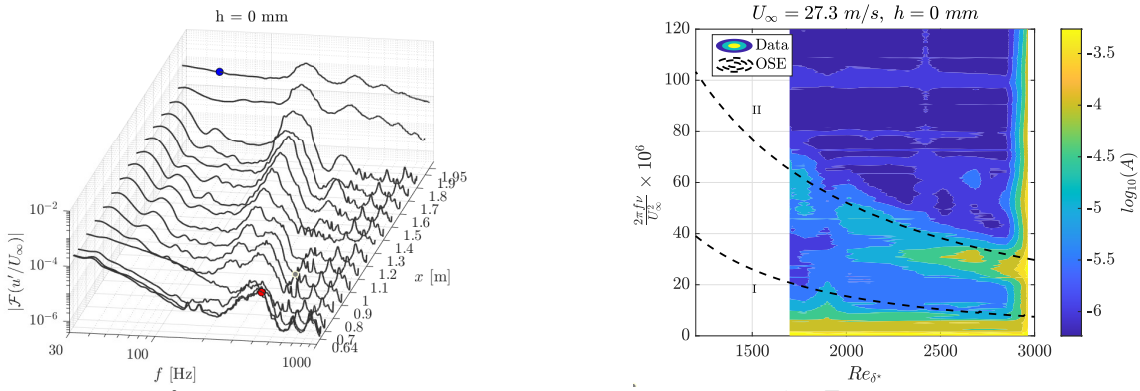

a). $f = 51 \Leftrightarrow 432$ Hz b). $F = 7.7 \Leftrightarrow 66.3$

Figure 14: Three dimensional spectra velocity and instability diagram for $h/\delta_h^\star = 0$.

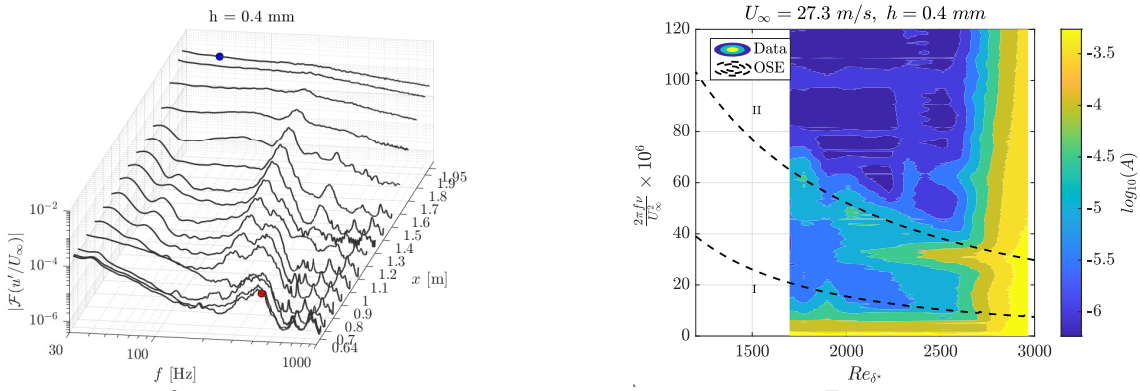

a). $f = 51 \Leftrightarrow 432$ Hz b). $F = 7.7 \Leftrightarrow 66.3$

Figure 15: Three dimensional spectra velocity and instability diagram for $h/\delta_h^\star = 0.36$.

3.3 A function that maps transition behavior caused by roughness elements

It will be shown an important results, which the collapse of the experimental data onto a hyperbolic curve established by Tani and Hama (1945), determining that a constant value equal to 320, and where x_{h_c} is the circular roughness location, h_c the diameter of the circular element and finally x_t is a transition point, this expression is given by Eq. 1:

$$Re_t = 320 \times \left(\frac{x_{h_c}}{h_c}\right)^{8/7} \left(\frac{x_t}{x_{h_c}}\right)^{3/7}, \tag{1}$$

it coincides with the data acquired in this work, with a difference of a coefficient of 0.48 that multiplies the height of the rectangular bump h_r, since in his case it is circular, resulting Eq. 2 as follows:

$$Re_t = 320 \times \left(\frac{x_{h_r}}{0.48 \cdot h_r}\right)^{8/7} \left(\frac{x_t}{x_{h_r}}\right)^{3/7}, \tag{2}$$

It is suspected that there is an effect of the wake due to the trailing edge of the rectangular bump, which could cause this difference. However, there is still no definitive conclusion. Figure 16 shows the collapse of the results at each velocity onto the hyperbolic curve, both for cases where $x_t/x_h < 1.1$ and $x_t/x_h > 1.1$.

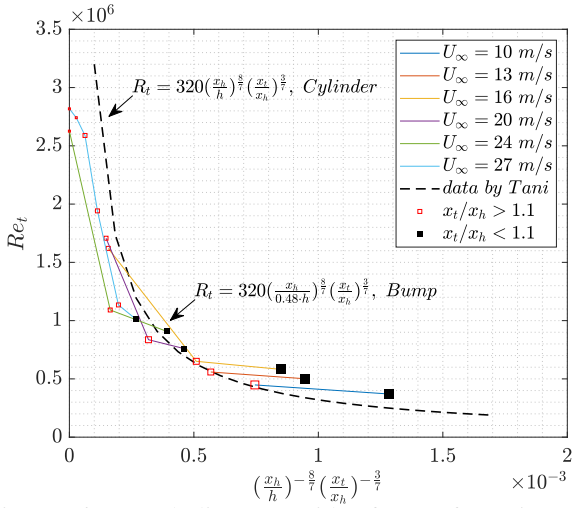

Figure 16: Hyperbolic curve with a factor of 0.48 in the rectangular bump height.

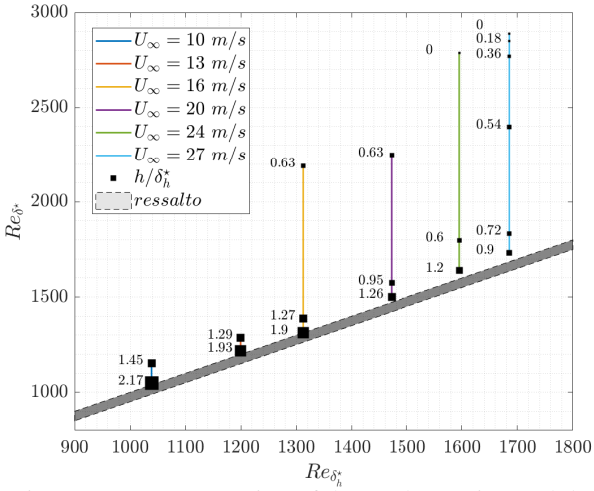

Figure 17: Representation of the total experimental data.

To provide a representation that include all the collected experimental data, Fig. 17 offers a visualization of these data. On the horizontal axis, we have the Reynolds delta star at the bump location, $Re_{\delta^\star_h}$, for each velocity, while on the vertical axis, we have the Reynolds number delta star for each transition point, $Re_{\delta^\star}$. Additionally, the sizes of the black symbols represent the bump height that cause transition, non-dimensionalized by the boundary layer displacement thickness at the rectangular element position at $x = 0.63$ m. Observing the non-dimensional values, it is evident that this is a suitable choice for understanding the relationship between the bump height and the boundary layer thickness. For values of $h/\delta^\star_h > 1$, the low velocity cases of 10 m/s and 13 m/s show that transition occurs very close to the roughness element, we see the impact in these two cases was moderate. Furthermore, there are values that are very close to each other; for example, for velocities $U = 16$ m/s and $U = 20$ m/s, both share the value of $h/\delta^\star_h = 0.63$.

3.4 Quadratic behavior of T-S wave growth respect to the bump height

Numerical results, provided by Himeno (2023), reveal a quadratic increase in the dimensionless magnitude of $h/\delta^\star$ relative to $\ln(A_{TS_h}/A_{TS_{h=0}})$, where h is the height of the rectangular step, $\delta^\star$ is the displacement thickness of the boundary layer, A_{TS_h} is the maximum amplitude around the dominant frequency of the T-S wave for each bump height, and finally, $A_{TS_{h=0}}$ represents the amplitude around the dominant frequency in the smooth case.

These results, shown in Fig. 18, a parabolic behavior of the small rectangular bump height relative to the maximum amplitude of the T-S band. It was shown that for a fixed station at $x = 950$ mm, the bands increase proportionally up to a value of $h/\delta^\star = 0.4$, corresponding to $(h/\delta^\star)^2 = 0.16$. Experimentally, it was found that for different stations and frequencies, the values that best fit are at the station $x = 1600$ mm with a frequency of $f = 205$ Hz. By squaring this dimensionless quantity, Fig. 19, we can observe a linear trend that coincides with the dashed reference curve.

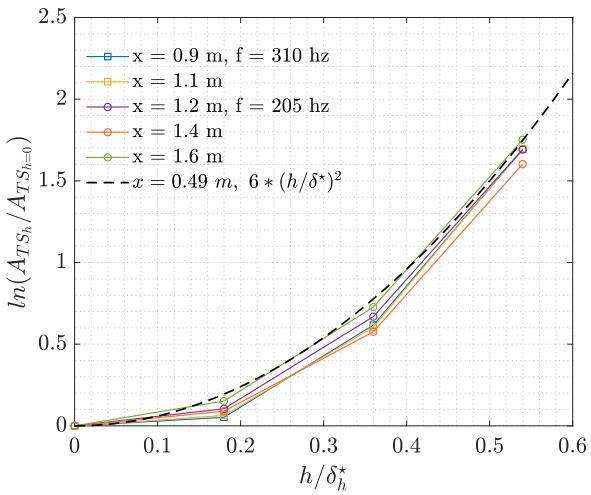

Figure 18: Parabolic behavior of the bump height with respect to the amplification rate of the T-S bands.

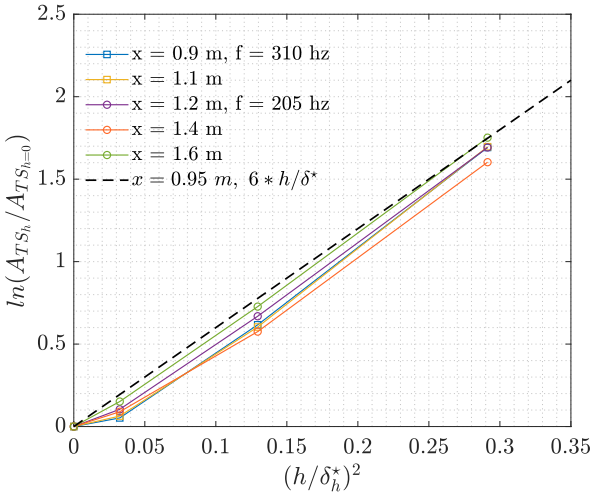

Figure 19: Linear behavior of the bump height with respect to the amplification rate of the T-S bands.

We also noticed that in this case, with a free stream velocity of 27.44 m/s, the curves maintained very similar slopes. However, when varying the Reynolds number in relation to velocity, it is estimated that the slopes of the curves would change, with higher or lower derivatives depending on the experimental conditions, given that the frequency ranges of the unstable region in the O-S instability diagram would be different. More graphs could have been obtained with the other velocity cases, but due to inadequate discretization, it was not possible to obtain a progressive evolution of the T-S waves.

3.5 The amplification factor

Finally, we conclude with a comparison of the envelope of the maximum amplitudes of the dominant frequency of the T-S waves, supported by the N-factor amplification theory. Due to the boundary layer growth too much before the bump position at $x = 600$ mm, the experimental data were shifted by adding a value of 3.2 on the y-axis, with the intention of match the theoretical curve that start at $x = 200$ mm with the experimental data. In this way, we aligned the data, observing a certain parallelism with the numerical curve. Theoretically, we obtained this curve from the solution of the Orr-Sommerfeld equations. This code was developed by a group, based on Juniper *et al.* (2014). The amplification ratio is integrated according to the Eq. 3:

$$N_{TS}(x) = \ln\left(\frac{A}{A_0}\right) = \max_{\alpha_i(w)}\left[-\int_{x_0}^{x} \alpha_i(x;w)dx\right], \tag{3}$$

In the integration for each x, the amplification ratio α_i was used as a function of the non-dimensional frequency $w = 2\pi f\delta^\star/U_\infty$. For this comparison, we restricted the frequency range between 100 and 560 Hz, corresponding to the frequencies within the unstable region of the instability diagram.

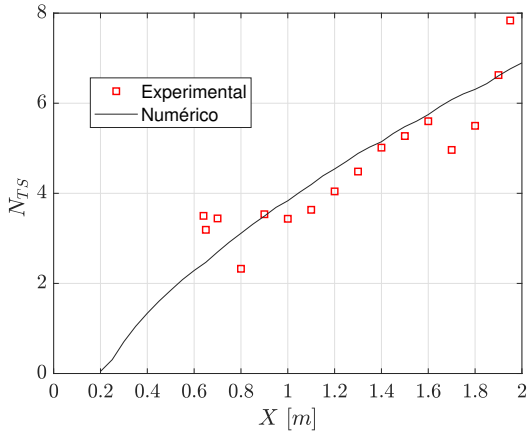

Figure 20: Comparison between the theoretical and experimental N-factor envelope for smooth case of 27.3 m/s.

Although the data does not coincide well with the experimental curve, it is important to clarify that due to various factors in the measurements, there may be experimental errors at some stations. During the positioning on the y-axis, considering 40% of the free-stream velocity, issues with the sealing of the test section may have occurred, causing recirculation or unfavorable pressure gradients.

4. CONCLUSION REMARKS

It is important to mention that there is a notable impact on the increase in the height of a rectangular bump on the amplification of Tollmien-Schlichting waves. However, we can also separate this effect into two regimes: the T-S Regime and the Bypass Transition Regime.

The measurements conducted with the Preston tube were crucial in determining the transition locations, ensuring that there was agreement with the hot-wire anemometry method, which were compared throughout this work. It was demonstrated that the transition behavior from laminar to turbulent can be represented by simple expressions, relating the transition Reynolds number and the dimensionless bump height with the boundary layer displacement thickness. These results revealed that, as shown in Fig. 16 and Fig. 17, for the maximum speed where natural transition occurs, there is a range where the impact of small bump heights is minimal, as well as for low free stream velocities.

Regarding the results shown in N-Factor (Fig. 20), the signal acquisition will be performed with more rigor, ensuring that the probe in y is in the correct position, avoiding any occurrence. One comparison not addressed in this work relates to ΔN, which correlates the transition N caused by the height of each rectangular bump, as shown in the works of Wang and Gaster (2005) and Crouch and Kosorygin (2020). Therefore, this will also be reviewed in later works.

5. ACKNOWLEDGEMENTS

L.J.L.L. and V.B.V. thank the Coordenação de Aperfeiçoamento de Pessoal de Nível Superior (CAPES) for the doctoral and master's scholarships. M.A.F.M. acknowledges support from Conselho Nacional de Desenvolvimento Científico e Tecnológico (CNPq) under grant number 307956/2019-9, Agência de Financiamento de Estudos e Projetos (FINEP) under grant number 01-09-0334-04, Fundação de Amparo à Pesquisa do Estado de São Paulo (FAPESP) under grant number 2019/15336-7, The Boeing Company under grant number 2021-GT-353, and the US Air Force Office of Scientific Research (AFOSR) under grants FA9550-18-1-0112 and FA9550-23-1-0030, managed by Dr. Roger Greenwood.

6. REFERENCES

Amaral, F.R., 2021. "The low acoustic noise and turbulence wind tunnel of the university of sao paulo". *The Aeronautical Journal*, Vol. 126, pp. 1–33. doi:10.1017/aer.2021.80.

Crouch, J.D. and Kosorygin, V.S., 2020. "Surface step effects on boundary-layer transition dominated by tollmien–schlichting instability". *AIAA Journal*, Vol. 58, pp. 2943–2950. doi:10.2514/1.J058518. URL `https://doi.org/10.2514/1.J058518`.

Drela, M. and Giles, M., 1987. "Viscous-inviscid analysis of transonic and low reynolds number airfoils". *Aiaa Journal - AIAA J*, Vol. 25, pp. 1347–1355. doi:10.2514/3.9789.

Dryden, H.L., 1953. "Review of published data on the effect of roughness on transition from laminar to turbulent flow". *National Advisory Committee for Aeronautics*, pp. 477–482.

Gaster, M., 1990. "The nonlinear phase of wave growth leading to chaos and breakdown to turbulence in a boundary layer as an example of an open system". *Proceedings of the Royal Society of London Series A*, Vol. 430, No. 1878, p. 3–24. doi:org/10.1063/1.5131577.

Hanson, R.E., Buckley, H.P. and Lavoie, P., 2012. "Aerodynamic optimization of the flat-plate leading edge for experimental studies of laminar and transitional boundary layers". *Experiments in fluids*, Vol. 53, pp. 863–871.

Himeno, F.H., 2023. *On surface bumps and boundary layer transition*. Ph.D. thesis, Universidade de São Paulo.

Juniper, Matthew, P., Hanifi, A. and Theofilis, V., 2014. "Modal Stability Theory: Lecture notes from the FLOW-NORDITA Summer School on Advanced Instability Methods for Complex Flows, Stockholm, Sweden, 2013". *Applied Mechanics Reviews*, Vol. 66, No. 2, p. 024804. ISSN 0003-6900. doi:10.1115/1.4026604. URL `https://doi.org/10.1115/1.4026604`.

Klebanoff, P.S. and Tidstrom, K.D., 1972. "Mechanism by which a twodimensional roughness element induces boundarylayer transition". *The Physics of Fluids*, Vol. 15, p. 1173–1178.

Morkovin, M.V., 1985. "Bypass transition to turbulence and research Desiderata". In *In NASA. Lewis Research Center Transition in Turbines*. pp. 161–204.

Preston, J.H., 1954. "The determination of turbulent skin friction by means of pitot tubes". *The Journal of the Royal Aeronautical Society*, Vol. 58(518), p. 109–121. doi:doi:10.1017/S0368393100097704.

Reneaux, J., 2004. "Overview on drag reduction technologies for civil transport aircrafts". In *European Congress on Computational Methods in Applied Sciences and Engineering ECCOMAS 2004*.

Reshotko, E., 2001. "Transient growth: A factor in bypass transition". *Physics of Fluids*, Vol. 5, No. 13. doi: doi:10.1063/1.1358308.

Schlichting, H., 1933. "Laminare strahlausbreitung". *ZAMM - Zeitschrift Für Angewandte Mathematik Und Mechanik*, Vol. 13(4), p. 260–263. doi:10.1002/zamm.19330130403.

Schneider, W., 2001. "The importance of aerodynamics in the development of commercially successful transport aircraft". *Aerodynamic Drag Reduction Technologies*, pp. 9–16. doi:$10.1007/978 - 3 - 540 - 45359 - 8_2$.

Schrauf, G., 2005. "Status and perspectives of laminar flow". *The Aeronautical Journal*, Vol. 109, No. 1102, p. 639–644. doi:10.1017/S000192400000097X.

Schubauer, G.B. and Skramstad, H.K., 1947. "Laminar boundary layer oscillations and transition on a flat plate". *Journal of research of the National Bureau of Standards*, Vol. 38, p. 251.

Smith, A.M.O. and Gamberony, N., 1956. "Transition, pressure gradient and estability theory". *Douglas Aircraft Company, El Segundo Division*.

Stuper, J., 1949. "The influence of surface irregularities on transition with various pressure gradients". *Division of Aeronautics, Australia*, Vol. 9.

Tani, I. and Hama, R., 1945. "Experiments on the permissible roughness in the laminar boundary layer over a flat plate (in japanese)". *Wartime Research Report I—4*.

Tani, I., Hama, R. and Mituisi, S., 1940. "On the permissible roughness in the laminar boundary layer". *JAero. Res. Inst. Tokyo*.

Tollmien, W., 1928. "Über die entstehung der turbulenz. 1. mitteilung". *Nachrichten von der Gesellschaft der Wissenschaften zu Göttingen, Mathematisch-Physikalische Klasse*, Vol. 1929 (1928), pp. 21–44. URL `http://eudml.org/doc/59276>`.

van Ingen, J.L., 1956. "A suggested semi-empirical method for the calculation of the boundary layer transition region". *Delft University of Technology*.

Wang, Y.X. and Gaster, M., 2005. "Effect of surface steps on boundary layer transition". *Experiments in Fluids*, Vol. 39(4), p. 679–686. doi:10.1007/s00348-005-1011-7.

7. RESPONSIBILITY NOTICE

The following text, properly adapted to the number of authors, must be included in the last section of the paper: The author(s) is (are) the only responsible for the printed material included in this paper.